Articles

Structural Characterization of a (+)-*trans-anti*-Benzo[*a*]pyrene−DNA Adduct Using NMR, Restrained Energy Minimization, and Molecular Dynamics†

Matthew A. Fountain and Thomas R. Krugh*

Department of Chemistry, University of Rochester, Rochester, New York 14627

Received October 10, 1994; Revised Manuscript Received December 30, 1994®

ABSTRACT: The (+)-*trans-anti*-benzo[*a*]pyrene adduct formed at the N2 amino group of guanine is the major adduct found after metabolic activation of the ubiquitous carcinogen benzo[*a*]pyrene. The carcinogenic and mutagenic properties of the (+)-*trans-anti*-BP adduct, as well as related adducts, have been extensively studied. A DNA duplex containing a (+)-*trans-anti*-benzo[*a*]pyrene adduct covalently attached to the G8 nucleotide in the sequence d(CCTATGT[BP-G]CAC)·d(GTGCACATAGG) was synthesized and the structure characterized by one- and two-dimensional NMR spectroscopy, in conjunction with energy minimization and molecular dynamics. This BP-11-mer duplex exhibits NOESY cross-peaks between benzo[*a*]pyrene protons and BP-G8, C9, A16, and C17 nucleotide protons that clearly delineate the location of the BP moiety in the minor groove of a B-type duplex with the pyrene ring oriented toward the 5′ end of the modified strand. Large upfield shifts of A16 and C17 sugar resonances in the partner strand show that the pyrene moiety is situated near these sugars. Analysis of the spectra was complicated by the presence of chemical exchange line broadening of protons located near the (...T[BP-G]C...)·(...GCA...) adduct site which shows the presence of a minor conformation for this BP-modified duplex in which TA is the 5′ neighboring base pair. Distance restraints determined from NOESY spectra recorded at 20 °C were used in restrained and unrestrained energy minimization and molecular dynamics simulations to obtain a structure characteristic of the predominant conformation of the BP-11-mer duplex. The important structural features of the BP-11-mer are similar to those reported by Cosman et al. [(1992) *Proc. Natl. Acad. Sci. U.S.A. 89,* 1914−1918] for a (+)-*trans-anti*-BP adduct at a (...C[BP-G]C...)·(...GCG...) sequence in which CG is the 5′ neighboring base pair. No evidence of a conformational equilibrium was reported in this duplex, from which we conclude that the presence of a 5′ TA base pair plays a role in the conformational equilibrium. Watson−Crick base pairing is retained in the predominant conformer of the (+)-*trans-anti*-BP modified duplex, which provides a visualization of a structure that could allow faithful replication. The exchange rate could not be slowed sufficiently to allow individual distance parameters to be obtained for the minor conformer. We suggest, however, by analogy to the conformational equilibrium observed in an aminofluorene-modified duplex [Eckel, L. M., & Krugh, T. R. (1994) *Nature Struct. Biol. 1,* 89−94] that the minor conformer may involve disruption of base pairing at the adduct site to allow stacking of the BP moiety with adjacent base pairs.

Metabolites of the ubiquitous environmental pollutant benzo[*a*]pyrene (BP) are carcinogenic and mutagenic agents (Gelbion, 1980; Conney, 1982; Thakker et al., 1985; Glatt et al., 1986; Galat, 1990; Harvey, 1991); for a recent minireview see Jernstrom and Graslund (1994). Adducts from the reaction of (+)-*anti*-7,8-dihydroxy-9,10-epoxy-benzo[*a*]pyrene [(+)-*anti*-BPDE] are considerably more carcinogenic and mutagenic for mammalian cells than (−)-*anti*-BPDE, which is more mutagenic for bacterial cells (Conney, 1982; Burgess et al., 1985; Thakker et al., 1985). The C^{10} of (+)-*anti*-BPDE, located in the bay region, forms covalent linkages to guanine and adenine (Osborne et al., 1981). The predominant adduct of (+)-*anti*-BPDE involves a covalent bond between the exocyclic N^2 amino group of guanine and the C^{10} benzylic carbon of (+)-*anti*-BPDE (Figure 1) through *trans* opening of the epoxide ring, while (−)-*anti*-BPDE affords a mixture of *trans* and *cis* products (Pulkrabek et al., 1979; Cheng et al., 1989).

Structural characterization of BP−DNA adducts using optical methods shows that BP−DNA adducts exhibit two families of structures referred to as type I and type II adducts [e.g., Jernstrom and Graslund (1994)]. In type I adducts the BP moiety is believed to be intercalated or quasi-intercalated in the DNA helix, while in type II adducts the BP moiety is believed to be in an external position accessible to the solvent. While the present work was in progress, energy-minimized structures based on NMR-derived distance restraints have appeared for a (+)-*trans-anti*-BP-G, a (−)-*trans-anti*-BP-G, and a (+)-*cis-anti*-BP-G adduct embedded within DNA 11-mer duplexes from collaborative studies involving the Broyde, Geacintov, Harvey, and Patel groups (Cosman et al., 1992, 1993; de los Santos et al., 1992). In their (+)-*trans-anti*-BP structure (Cosman et al., 1992), the

† This publication was supported by Grant CA35251 from the National Cancer Institute. Its contents are solely the responsibility of the authors and do not necessarily represent the official views of the National Cancer Institute.

® Abstract published in *Advance ACS Abstracts,* February 15, 1995.

0006-2960/95/0434-3152$09.00/0

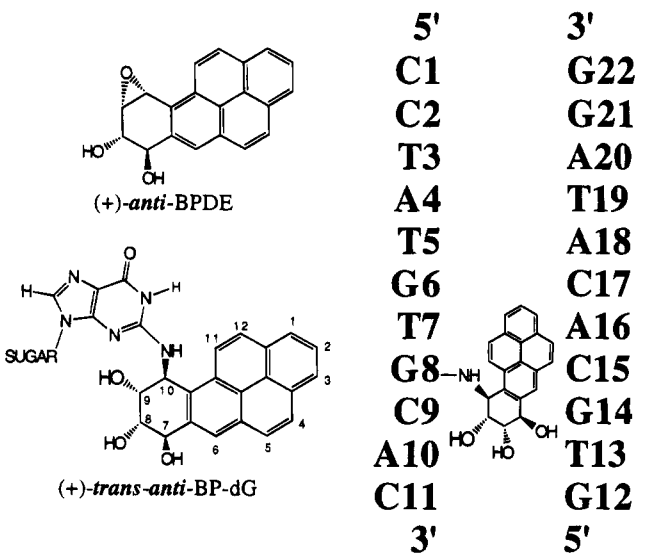

FIGURE 1: Chemical structures of the (+)-*anti*-benzo[*a*]pyrene diol epoxide and the (+)-*trans-anti*-BP−dG adduct and a representation of the sequence of the BP-11-mer in which the BP moiety is covalenty attached at the N^2 of G8.

BP-modified guanine has cytosine as both the 5′ and 3′ neighbors [that is, the (+)-*trans-anti*-BP adduct was embedded within a (...C[BP-G]C...)•(...GCG...) sequence]. We report below on a BP-modified duplex in which a (+)-*trans-anti*-BP adduct is bound at a (...T[BP-G]C...)•(...GCA...) sequence.

Mutagenic studies show that the (+)-*trans-anti*-BP adducts exhibit mutation preferences that are affected by the adjacent 5′ nucleotide (Mackay et al., 1992; Rodriguez & Loechler, 1993a,b; Shibutani et al., 1993). For example, when a transversion mutation occurs at a d(...T[BP-G]C...) lesion, GC to TA transversions are produced exclusively, while d(...A[BP-G]C...), d(...G[BP-G]C...), and d(...C[BP-G]C...) lesions exhibit mixtures of GC to TA, GC to CG, and GC to TA mutations (Mackay et al., 1992). These mutagenesis studies support the need to determine the impact of DNA sequence on adduct structure.

We use two-dimensional NMR spectroscopy to characterize the structure of the deoxyoligonucleotide duplex d(CCTATGT[BP-G]CAC)•d(GTGCACATAGG), hereafter called the BP-11-mer, where BP-G is a (+)-*trans-anti*-BP-G adduct (Figure 1) embedded within a (..T[BP-G]C..) sequence on the modified strand (Figure 1). The modified strand contains two guanines, which after reaction with racemic (±)-*anti*-BPDE yields at least four products that were successfully separated by reverse-phase chromatography. We show below that the BP-11-mer exists as an equilibrium involving at least two different conformations, one of which predominates in solution. The structure of the predominant conformation has been characterized by energy minimization using distance restraints from NOESY spectra. In this (+)-*trans-anti*-BP-modified duplex the BP moiety is in the minor groove and is oriented toward the 5′ end of the modified strand. Thus the predominant conformer has a structure that is consistent with that observed independently by Cosman et al. (1992) for binding of (+)-*trans-anti*-BP at a d(...C[BP-G]C...) sequence and as predicted in computational studies (Singh et al., 1991). These duplexes retain Watson−Crick pairing for all base pairs and thus provide a visualization of a conformation that might allow faithful replication.

Our laboratory recently characterized an aminofluorene-(AF-) modified duplex (Eckel & Krugh, 1994a,b) and found that the fluorene moiety was in equilibrium between external and inserted conformations [also see Cho et al. (1994)]. Although the aminofluorene-modified duplexes represent a different system, the conformational equilibrium observed in this system provides insight in the present experiments. In the external conformation the aminofluorene-modified guanine retains Watson−Crick base pairing, while in the inserted conformer the AF-G pairing with its partner C was disrupted to allow for stacking of the fluorene moiety with adjacent base pairs. In the aminofluorene-modified duplex the two conformers could be characterized independently because at low temperatures (5 °C) interconversion between the two conformers was slow compared to the NOESY mixing time. For the BP-11-mer, however, the rate of interconversion between conformers could not be sufficiently slowed to allow direct characterization of the minor conformer.

By analogy to the aminofluorene system, we suggest as a working hypothesis that a likely candidate for the minor conformer involves disruption of the BP-modified base pair to allow stacking of the hydrophobic BP moiety with adjacent base pairs, as observed for a (+)-*cis-anti*-BP-modified duplex (Cosman et al., 1993) and in the recently reported solution conformation of a (+)-*trans-anti*-BP-modified duplex in which the BP-G moiety is opposite a deletion (Cosman et al., 1994).

MATERIALS AND METHODS

The oligodeoxynucleotides d(CCTATGTGCAC) and d(GTGCACATAGG) were synthesized using the phosphoramidite method on a Gene Assembler Plus DNA synthesizer (Pharmacia). Optically active (+)-*anti*- and (−)-*anti*- as well as racemic (+)-*anti*-benzo[*a*]pyrene 7,8-dihydrodiol 9,10-epoxides were purchased from Chemsyn Science Laboratory, Lenexa, KS, and NCI Chemical Carcinogen Reference Standard Repository, Kansas City, MO.

Purification of Oligonucleotides. Oligonucleotides were purified by thin-layer chromatography on Baker-analyzed silica gel (Si500F, 20 cm × 20 cm) plates with a fluorescent indicator using 55% 1-propanol, 35% ammonium hydroxide, and 10% water as the mobile phase (Chou et al., 1989). The purity of each oligonucleotide was checked by HPLC using a Varian 5000 LC with a PRP-1 reverse-phase semipreparative column (305 mm × 7 mm i.d.) with a 10-μm sphere size (Hamilton, Reno, NV). The column was eluted with the following solvent system: 70% acetonitrile:10% methanol: 20% 0.01 M potassium phosphate, pH 7.0, as the organic phase, and 0.01 M potassium phosphate, pH 7.0, as the aqueous phase. A bilinear gradient was used, going from 5% to 20% organic solvent in 30 min and then to 100% organic solvent in 10 min, with a flow rate of 2.0 mL/min. The HPLC chromatograms were recorded and analyzed using Dynamax HPLC Method Manager (Rainin Instrument Co. Inc.). The eluant was monitored by a Varian 2550 variable-wavelength detector set at 260 nm. After HPLC, the oligonucleotides were concentrated and desalted using Sep-pak C18 cartridges, (Waters Inc.) and then lyophilized to dryness.

Formation of BP Adducts. The d(CCTATGTGCAC) oligodeoxynucleotide was dissolved in 0.1 M sodium chlo-

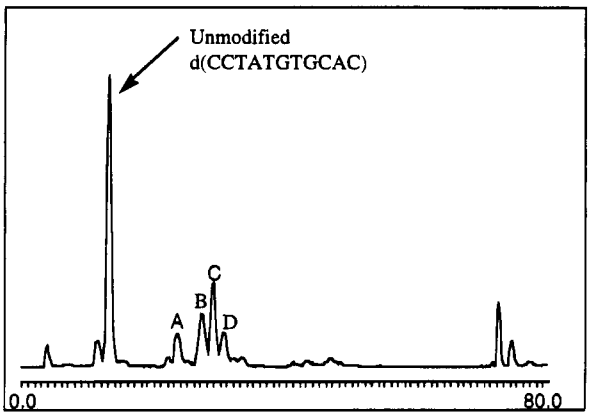

FIGURE 2: HPLC elution profile of the reaction mixture of the oligonucleotide d(CCTATGTGCAC) with racemic (±)-*anti*-BPDE. The gradient was from 5% to 25% organic solvent in 60 min and then to 100% in 10 min, using 70% acetonitrile:10% methanol: 20% 0.01 M potassium phosphate (pH 7.0) as the organic solvent and 0.01 M potassium phosphate (pH 7.0) as the aqueous solvent.

ride and 0.01 M sodium phosphate buffer, pH 7.0, to give a DNA concentration of 0.5 mM. Racemic (±)-*anti*-BPDE was dissolved in anhydrous tetrahydrofuran to give a 0.0165 M BPDE stock solution. The BPDE stock solution was added in 100-μL aliquots to the DNA solution until the final ratio of BPDE to DNA was 3:1. The reaction was mixed for 5 min between aliquots and then overnight with a magnetic stir bar. After the reaction was complete, the reaction mixture was centrifuged to pellet precipitated benzo-[*a*]pyrene tetraol and then extracted several times with ether to remove any unreacted BPDE and BP tetraol prior to HPLC purification. The same HPLC solvents used in DNA purification were also used to separate the BP−DNA oligomers with a bilinear gradient from 5% to 20% organic solvent in 30 min and then 20% to 100% organic solvent in 10 min with a flow rate of 2.0 mL/min. The BP oligomers were subjected to another round of HPLC using the same solvents as described above, with a bilinear gradient from 5% to 25% organic solvent in 60 min and then to 100% in 10 min with a flow rate of 2.0 mL/min. A chromatogram showing the separation is shown in Figure 2.

Adduct Characterization. Ultraviolet absorption spectra were recorded on a Varian Cary 219 spectrophotometer, and circular dichroism spectra were recorded on a Jasco J40 CD spectropolarimeter in 0.1 M sodium chloride, 0.01 M sodium phosphate, and 0.001 M EDTA buffer solution at pH 7.0. The UV absorbance at 350 and 260 nm was used to show formation of a 1:1 BP:d(CCTATGTGCAC) adduct. A comparison of the UV and CD spectra of adducts labeled as A and C in Figure 2 (Figure S1, in the supplementary material) to those reported previously (Cheng et al., 1989; Cosman et al., 1990; Geacintov et al., 1990) shows that adduct A is a (−)-*trans-anti*-BP-dG-modified oligomer and adduct C is a (+)-*trans-anti*-BP-dG-modified oligomer. Approximately 50% of the oligonucleotide formed covalent adducts, of which approximately 22% was a (+)-*trans-anti*-BP-dG-modified oligomer and 18% was a (−)-*trans-anti*-BP-dG-modified oligomer; the remainder was a mixture of stereoisomers.

The (+)-*trans-anti*-BP-modified duplex has a T_m of 42 °C (1 μM), which is 13 °C lower than the T_m of 55 °C for the unmodified 11-mer. The T_m for the BP-11-mer at NMR concentrations is greater than 50 °C (Fountain, 1994).

NMR Sample Preparation. One equivalent of the complementary d(GTGCACATAGG) oligodeoxynucleotide was added to the d(CCTATGT[BP-G]CAC) oligodeoxynucleotide, and the mixture was dissolved in 500 mL of 0.1 M sodium chloride, 0.01 M sodium phosphate, pH 7.1, and 0.1 mM EDTA in 99.996% D_2O solution. Trimethylsilylpropionate-*2,2,3,3-d*$_4$ (TSP) was added to the NMR sample as a chemical shift reference. The sample was lyophilized to dryness and dissolved in 500 μL of 99.996% D_2O, giving a d(CCTATGT[BP-G]CAC)·d(GTGCACATAGG) duplex concentration of 1.1 mM. For NMR experiments in H_2O solution, the sample was dissolved in 500 μL of 90% H_2O: 10% D_2O. The sample was degassed under vacuum, placed in a clean NMR tube, and purged with argon.

NMR Experiments. A Varian VXR 500S NMR spectrometer operating at 499.8 MHz was used for all 1D and 2D NMR experiments. NMR data were processed using Varian VNMR software on SUN 3 and SUN 4 workstations and with FELIX 2.10 software on an Silicon Graphics, Inc., workstation.

NOESY spectra were recorded using the standard (90°−t_1−90°−mix−90°−acquire)$_n$ pulse sequence consisting of 256 t_1 increments, each having 4K points with 64 scans per fid and a recycle delay time of 3 s. The residual HOD peak was suppressed by irradiation during the recycle delay time. The data were zero filled to 2K data points in the t_1 dimension to yield a 4K by 2K matrix. The data were apodized with a shifted sine bell squared function in both dimensions.

TOCSY spectra were recorded using the standard (90°−t_1−spin lock−acquire)$_n$ pulse sequence consisting of 256 t_1 increments, each having 4K data points with either 64 or 96 transients per fid with a recycle delay time of 3 s and spin-lock mixing time of 50 ms. The residual HOD peak was suppressed by irradiation during the recycle delay time. The data were zero filled to 2K data points in the t_1 dimension to yield a 4K by 2K matrix. The data were apodized with a phase-shifted sine bell squared function in both dimensions.

DQF-COSY spectra were acquired by the standard (90°−t_1−90°−t−90°−acquire)$_n$ pulse sequence consisting of 512 t_1 increments, each having 4K data points. Typical data sets consisted of 64 or 96 scans per fid, with a 2.5-s recycle delay time. The data were apodized with a 90° phase-shifted sine bell squared function in both dimensions.

Phase-sensitive NOESY experiments in H_2O were recorded with 100- and 150-ms mixing times at 10 and 1 °C, with a 1−1-echo water suppression pulse sequence replacing the last 90° pulse in the NOESY pulse sequence (Sklenar & Bax, 1987). A sweep width of 12 000 Hz was used in both dimensions with delays used in the 1−1-echo water suppression pulses of 50 μs between the two 180° pulses and 80 μs for the echo delay. A total of 256 complex t1 increments each having 4K data points, were recorded using either 64 or 96 transients per t_1 increment and a recycle delay time of 3 s. The data were zero filled to 4K data points in the t_1 dimension to yield a 4K by 4K matrix. The data were apodized with a shifted sine bell squared function in both dimensions.

The one-dimensional NOE experiments in 90% H_2O:10% D_2O solution were recorded using a 1−3−3−1 binomial pulse sequence (Hore, 1983). One-dimensional NOE difference spectra were obtained by subtracting on-resonance

and off-resonance 1D spectra. Imino protons were saturated using the decoupler channel.

Exchange rates of imino protons were determined using published methods (Early et al., 1980; Mirau & Bovey, 1987). The spin−lattice relaxation rates were measured at −5 °C to minimize the exchange rates of the imino protons. A (180°−binom−delay−90°−binom−acquire)$_n$ pulse sequence with delay times ranging from 4 ms to 5 s was used to measure spin relaxation times. A 250-ms pulse on the decoupler channel prior to the 180° binomial pulse was used to invert the water resonance. A total of 512 transients were collected with a recycle delay of 3.5 s. The difference in the initial spin-lattice relaxation rates with and without inversion of the water resonances was used to determine the exchange rates (Early et al., 1980; Mirau & Bovey, 1987).

Computational Studies. Insight II version 2.1.0 and Discover version 2.8 (Biosym Technologies Inc.) software packages on a Silicon Graphics workstation were used for graphics display and for computations using the AMBER force field (Weiner et al., 1984, 1986; Singh et al., 1988). Calculations were done *in vacuo* with a distance-dependent dielectric constant of 4 and a cutoff distance of 15 Å. The BP-11-mer duplex was constructed using the Biopolymer module in Insight II. The atomic charges of the BP-G8 residue are those previously reported by Broyde and coworkers (Singh et al., 1991). The phosphate oxygen charges were reduced by 50%, giving each nucleotide a net charge of −0.1583. The starting conformation of the BP-11-mer duplex was B-form DNA. The BP chromophore was oriented toward the 5′-end of the modified strand as dictated by NOE and chemical shift data (see Results).

NOE-derived distances were calculated from the ratio of the volume of the cross-peak in question to the volume of C-H5 to C-H6 cross-peaks using the isolated spin pair approximation, where the NOESY cross-peak volume is inversely proportional to the distance raised to the sixth power. Distances were calculated from a 150-ms mixing time NOESY spectrum collected at 20 °C. The BP−DNA proton distances were referenced to the C15-H5/H6 and C17-H5/H6 cross-peak volumes. The lower and upper bounds for the BP-H9 to C9-H1′, BP-H10 to BP-G8-H1′, and BP-H10 to C9-H1′ distance restraints included ~30% error limits on their NOE-derived distances because of the relatively long mixing time used to determine the NOE distances. The lower and upper bounds for the BP-H6 to A16-H4′, BP-H5 to A16-H4′, BP-H11 to A16-2H, BP-H12 to A16-2H, and BP-H2 to C17-H4′ distances restraints were set to 2.0 and 5.0 Å to minimize the impact of chemical exchange on the apparent distances.

The distance restraint penalty function consisted of a five-section continuous function:

$$E = \begin{cases} E_1 + (R_1 - R_{ij})F_1 & R_{ij} < R_1 \\ K_2(R_{ij} - R_2)^2 & R_1 < R_{ij} \le R_2 \\ 0 & R_2 < R_{ij} \le R_3 \\ K_3(R_{ij} - R_3)^2 & R_3 < R_{ij} \le R_4 \\ E_1 + (R_{ij} - R_4)F_4 & R_4 < R_{ij} \end{cases} \quad (1)$$

where R_1 and R_4 are the distances where the harmonic potential becomes linear, R_2 is the lower bound distance, R_3 is the upper bound distance, R_{ij} is the current distance between the two atoms, and F_1, F_4, K_2, and K_3 are force constants. The force constants K_2 and K_3 ranged from 20 to 50 kcal mol^{-1} Å^{-2} for individual restraints, while F_1 and F_4 were set to 1000 kcal mol^{-1} Å^{-1} for all restraints. In addition to NMR-derived distance restraints (see Results), hydrogen bond restraints, using bounds of 1.7−2.2 Å, between each hydrogen bond donor and acceptor in each base pair were employed to ensure the Watson−Crick base pairing observed in the NMR spectra.

Calculations began with restrained energy minimization followed by restrained molecular dynamics (2 ps at 300 K, 2 ps at 500 K, and 2 ps at 300 K). After molecular dynamics, restrained energy minimization was resumed to provide an energy-minimized structure. The BP to DNA distance restraints were then removed, and energy minimization was performed again. The release of these restraints did not result in any significant structural changes.

RESULTS

Assignment of Exchangeable Protons. The imino and amino proton assignments for the BP-11-mer are shown in Table 1, and were obtained from one- and two-dimensional NOE experiments in 90% H_2O:10% D_2O buffer. All 11 imino protons are observed in the one-dimensional NMR spectrum at −5 °C (Figure 3A), although it is noteworthy that even at this low temperature the T7 imino proton is unusually broad. The T7-N3H proton (14.2 ppm) was assigned by an NOE to the G6-N1H proton. The BP-G8-N1H proton (12.20 ppm) was assigned by an NOE to the G14-N1H. An NOE between the T7-N3H and BP-G8-N1H protons was not observed, presumably due to exchange broadening. The T7-N3H resonance at 14.2 ppm broadens into the baseline at temperatures above 4 °C (Figure 3B). The BP-G8-N1H resonance (12.20 ppm) overlaps with the G6-N1H resonance (12.32 ppm) at higher temperatures, and thus the temperature dependence of the line width of the BP-G8-N1H proton could not be monitored (Figure 3B).

In the two-dimensional NOESY spectrum of the BP-11-mer recorded in H_2O solution (Figure 4), the T7-N3H and BP-G8-N1H protons exhibit exchange cross-peaks with the solvent (cross-peaks H and I in Figure 4), suggesting faster solvent exchange for the T7-N3H and BP-G8-N1H protons than for other internal imino protons. Although solvent exchange could explain the unusual line broadening observed with the T7 and BP-G8 imino protons, cross-peaks H and I are not especially large, suggesting that solvent exchange is not the most important factor resulting in the line broadening of the T7 and BP-G8 imino protons. To investigate this further, the relative exchange rates for the imino protons at −5 °C were measured using the method described by Mirau and Bovey (1987). These data (Figure S2, in supplementary material) show that the T7 and the BP-G8 imino protons have solvent exchange rates that are approximately 1.5 times larger than other thymine and guanine internal imino protons, respectively. This relatively modest increase in solvent exchange rate suggests that transient fraying and subsequent exchange with solvent protons that is observed in all DNA oligomers [e.g., Folta-Stogniew and Russu (1994)] are not sufficient to explain the unusual line broadening observed for the T7-N3H proton. We interpret this as evidence that the broadening is primarily a result of interconversion between a predominant conformer and a minor conformer (or conformers). Line broadening observed in other base

Table 1: Chemical Shift Values of the Nonexchangeable and Exchangeable Protons in the Predominant and Minor Conformations of the d(CCTATGT[BP-G]CAC)·d(GTGCACATAGG) Duplex[a]

base	TMe	H6/H8	H1'	H2''	H2'	H3'	H4'	H5'/H5''	2H	H5	imino	amino
C1		7.82	6.01	2.50	2.26	4.70	4.25			5.97		*b*
C2		7.69	6.04	2.50	2.18	4.85	4.25			5.70		8.36/7.0
T3	1.72	7.46	5.76	2.53	2.22	4.93	4.26				13.65	
A4		8.36	6.30	2.97	2.72	5.03	4.38		7.44			7.78/6.50
T5	1.48	7.12	5.79	2.42	2.10	4.86	4.11				13.35	
G6		7.66	5.89	2.69	2.50	4.87	4.35				12.32	
T7	1.28	7.20	5.95	2.42	2.05	4.90	4.40				14.2	
BP-G8		7.96	6.38	2.90	2.72	5.05	4.46				12.20	
C9		7.36	5.83	2.42	2.04	4.88	4.38			5.49		8.62/6.65
A10		8.27	6.30	2.86	2.70	5.02	4.44		7.90			*b*
C11		7.44	6.14	2.19	2.14	4.50	4.21			5.46		*b*
G12		7.97	6.05	2.78	2.67	4.84	4.25				12.87	*b*
T13	1.46	7.37	5.98	2.52	2.19	4.92	4.26				13.92	*b*
G14		7.58	5.82	2.60	2.60	4.96	4.36				12.65	
C15		7.11	5.48	1.98	1.64	4.63	4.12			5.11		*b*
A16		7.54	4.40[c]	1.22	1.69	4.40	3.38	3.95/3.95	7.40			*b*
C17		6.92	4.76	2.10	1.90	4.42	3.78	3.85/3.52		5.10		8.15/6.58
A18		8.13	6.22	2.89	2.57	4.98	4.46		7.44			7.92/6.39
T19	1.39	7.22	5.61	2.16	1.82	4.86	4.19		7.42		13.52	
A20		8.14	5.95	2.82	2.64	5.02	4.39					7.72/6.30
G21		7.65	5.66	2.64	2.50	4.96	4.36				12.36	
G22		7.70	6.12	2.64	2.42	4.61	4.05				13.22	

[a] Chemical shift assignments were recorded at 37 °C and referenced to TSP at 0.0 ppm. [b] Not observed due to exchange with the water resonance. [c] Assignment is tentative and may be exchange broadened into the baseline.

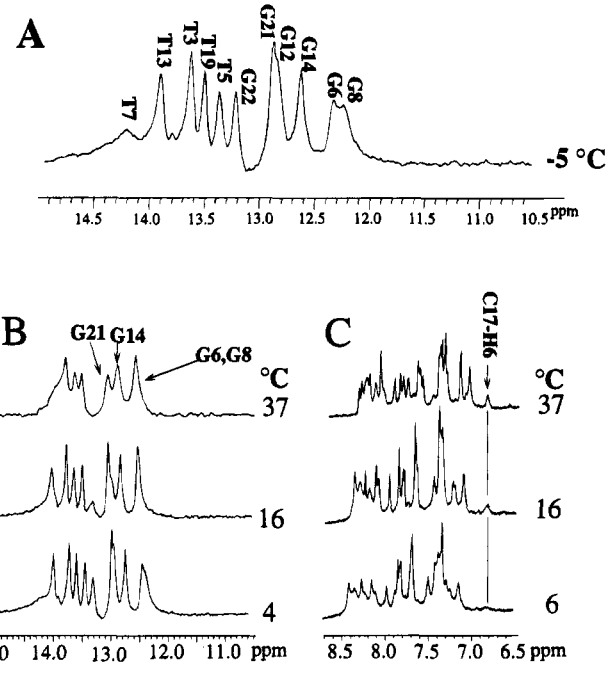

FIGURE 3: Portions of one-dimensional NMR spectra recorded at several temperatures: (A) the imino proton region recorded at −5 °C; (B) the imino proton region recorded at 4, 16, and 37 °C; (C) the base region recorded at 6, 16, and 37 °C showing the broadening of the C17-H6 resonance.

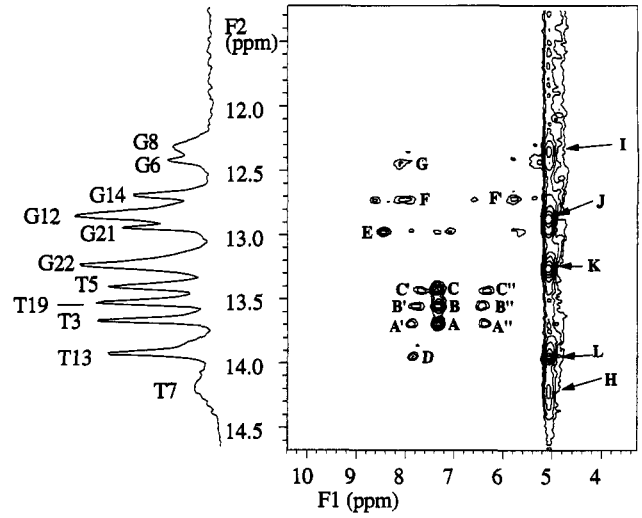

FIGURE 4: Portion of a two-dimensional NOESY spectrum of the imino proton region of the BP-11-mer duplex recorded at 1 °C with a 150-ms mixing time. The labeled cross-peaks are A, T3-N3H to A20-2H; A′ and A″, T3-N3H to A20-N6H$_2$ protons; B, T19-N3H to A4-2H; B′ and B″, T19-N3H to A4-N6H$_2$ protons; C, T5-N3H to A18-2H; C′ and C″ T5-N3H to A18-N6H$_2$ protons ; D, T13-N3H to A10-2H; E, G21-N1H to C2-N4H$_2$; F and F′, G14-N1H to C9-N4H$_2$ protons; G, G6-N1H to C17-N4H$_2$; H, T7-N3H to H$_2$O; I, G8-N1H to H$_2$O; J, G12-N1H to H$_2$O; K, G22-N1H to H$_2$O; and L, T13-N3H to H$_2$O.

and sugar proton resonances is consistent with this interpretation.

NOE interactions shown in Figure 4 establish Watson–Crick hydrogen bonding for 7 of the 11 base pairs. The two terminal base pairs (C1·G22 and C11·G12) and the T7 and BP-G8 imino protons did not exhibit cross-peaks between the imino proton and the amino proton of the partner base, and thus the hydrogen-bonding pattern for these bases could not be determined from these data. The chemical shifts of the T7 imino proton (14.2 ppm) and the BP-G8 imino proton (12.20 ppm) are in the expected regions for Watson–Crick thymine and guanine imino protons. The possibility of Hoogsteen hydrogen bonding for the T7·A16 and BP-G8·C15 base pairs was discounted because Hoogsteen hydrogen bonding requires that the purine adopt a *syn* conformation, and both the BP-G8-H8 and the A16-H8 protons exhibit medium-strength NOEs to their adjacent 3′ C-H5 proton (cross-peaks 1 and 2 in Figure 5), which is consistent with an *anti* conformation, as are the weak base to H1′ NOEs for the BP-G8 and the A16 nucleotides.

Interchangeable Conformations. The temperature dependence of the line width of the C17-H6 resonance (Figure 3C) establishes the presence of interconversion between two (or

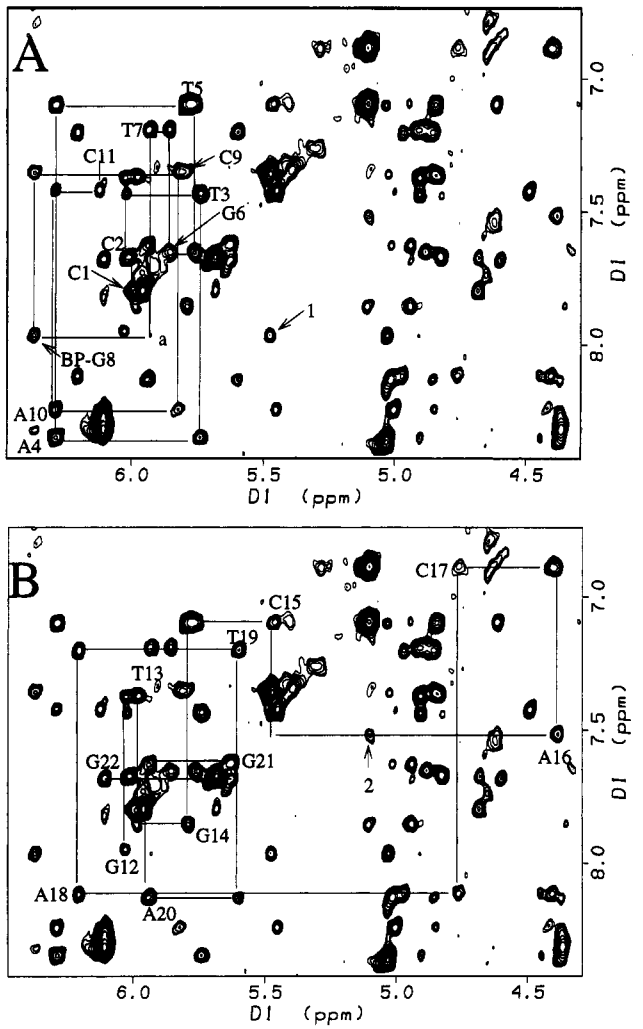

FIGURE 5: Base to H1′ proton region of a 400-ms NOESY spectrum recorded at 37 °C. The base to H1′ connectivities for the d(CCTATGT[BP-G]CAC)-modified strand (panel A) and the d(GTGCACATAGG) complementary strand (panel B) are shown. The cross-peak labels are as follows: 1, BP-G8-H8 to C9-H5; a, T7-H1′ to BP-G8-H8; 2, C17-H5 to A16-H8.

more) conformations. In NOESY spectra recorded at 5, 10, and 20 °C broadening is observed for the C15, A16, and C17 base and sugar proton resonances, as well as for BP proton resonances (Figure S3, in supplementary material). In the 10 °C NOESY spectra intranucleotide base to sugar NOEs were not observed for either the A16 or C17 nucleotides, and the C17-H5 to C17-H6 NOESY cross-peak was significantly broadened. In the 5 °C NOESY spectrum the C17-H6 to C17-H5 NOESY cross-peak was not observed, as expected from the one-dimensional NMR data (Figure 3C) where the C17-H6 resonance is very broad. The C15-H5 to C15-H6 cross-peak is also weak due to broadening. We interpret the selective broadening of resonances near the adduct site as evidence of equilibrium between a predominant conformer and a minor conformer (or conformers). Unfortunately, the interconversion between conformers could not be slowed sufficiently to observe cross-peaks corresponding to a second conformation.

Chemical Shift Assignments of Nonexchangeable Protons. Resonance assignments for the predominant conformer of the BP-11-mer were made by examination of NOESY, DQF-COSY, and TOCSY spectra, as described in detail by Fountain (1994). The base to H1' NOESY connectivities

Table 2: Benzo[*a*]pyrene Proton Chemical Shifts[a]

BP proton	chemical shift	BP proton	chemical shift
H1	8.32	H7	5.03
H2	8.12	H8	4.38
H3	8.33	H9	4.35
H4	8.20	H10	6.13
H5	8.19	H11	8.36
H6	8.36	H12	8.31

[a] Chemical shifts were recorded at 20 °C and referenced to TSP at 0.0 ppm.

for the modified strand, C1 to C11 (Figure 5A), and the partner strand, G12 to G22 (Figure 5B), can be traced without disruptions. All base and sugar protons (except H5′ and H5″ protons) were assigned at 37 °C and are listed in Table 1.

The base to H1′ NOE connectivities between the T7-H1′ and BP-G8-H8 protons in the modified strand, as well as the C15-A16-C17 base to H1′ NOE connectives in the partner strand, were weaker than expected for B-DNA, which may be due in part to exchange broadening. The A16-H8, A16-H1′, A16-H2′, and A16-H2″ protons exhibited sufficient line broadening such that the A16-H1′ proton, at 4.40 ppm, could only be tentatively assigned by NOESY or TOCSY cross-peaks to the A16-H2′/H2″ protons. The A16-H3′ proton also resonates at 4.40 ppm. As a result of the overlap, neither the A16-H1′ nor the A16-H3′ protons were used to calculate distance restraints.

Chemical Shift Assignments of Benzo[a]pyrene Protons. The BP protons were assigned by inspection of the NOESY, TOCSY, and DQF-COSY spectra at 20 °C and are given in Table 2. NMR spectra showing the assignments of the BP protons can be found in Figures S4 and S5, in supplementary material.

Chemical Shift Assignments of the Unmodified 11-mer Duplex. The chemical shifts of the exchangeable and nonexchangeable protons in the unmodified 11-mer were determined (Table S1, in supplementary material) to provide a comparison to the BP-11-mer assignments. Qualitative analysis of NOESY and TOCSY spectra indicates that the unmodified 11-mer adopts a right-handed B-type duplex.

Chemical Shift Changes upon Adduct Formation. A comparison of the chemical shifts of the base and sugar protons in the predominant conformer with those of the unmodified 11-mer are given in Figure 6. Relatively small $\Delta\delta$ values were observed in the modified strand, except for the BP-G8-H1′ proton which was downfield shifted −0.6 ppm (Figure 6A). In the partner strand, large upfield chemical shift changes were observed for the C15, A16, and C17 base and sugar protons (Figure 6B). The largest chemical shift changes were centered on the A16 sugar protons (e.g., A16-H2″, +1.7 ppm and A16-H2′, +1.3 ppm), with the C15 and C17 base and sugar protons exhibiting smaller upfield shifts (Figure 6B). The large upfield chemical shift changes observed in the partner strand indicate that the BP chromophore lies directly above the A16 and C17 sugars in the minor groove.

J-Coupling in the Benzylic Ring. The $J_{H10\text{-}H9}$ (9 Hz) and $J_{H8\text{-}H7}$ (5 Hz) coupling constants were measured in a DQF-COSY spectrum to provide data on the BP[H10-C10-C9-H9] and BP[H8-C8-C7-H7] dihedral angles. The large *J*-coupling between the BP-H8 and BP-H7 protons and the moderate *J*-coupling between the BP-H10 and BP-H9 protons

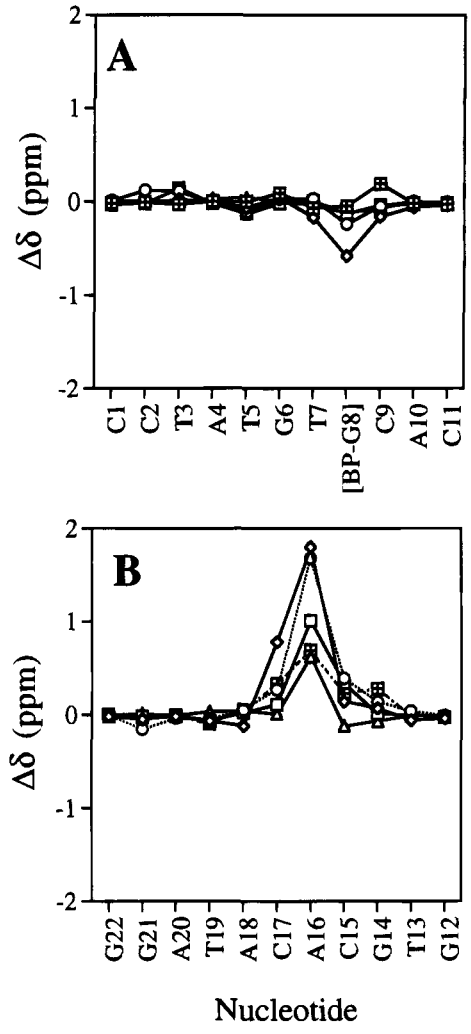

FIGURE 6: Graphs of the $\Delta\delta$ values between the BP-11-mer and the unmodified d(CCTATGTGCAC)·d(GTGCACATAGG) 11-mer duplex for the H8/H6, H1′, H2′, and H3′ protons: (A) graph of the $\Delta\delta$ values for the modified strand {d(C1-C2-T3-A4-T5-G6-T7-[BP-G8]-C9-A10-C11)}; (B) graph of the $\Delta\delta$ values for the partner srand {d(G12-T13-G14-C15-A16-C17-A18-T19-A20-G21-G22)}. Symbols used are H6/H8, □; H1′, ◇; H2″, ○; H2′, △; and H3′, crossed □.

indicate that the benzylic ring adopts a pseudo-chair conformation.

BP−DNA NOE Interactions for the Predominant Conformer. A total of 26 NOE cross-peaks were observed between BP protons and DNA protons, as shown in Table S2, in supplementary material. The BP to DNA NOEs span the entire BP moiety and define the orientation of the BP moiety in the minor groove. The BP-aliphatic to DNA proton NOEs show that BP is attached to the G8 base. This question arises because the BP-modified strand has two guanines and thus the reaction with racemic BP diol epoxide produced both (+) and (−) enantiomers at both G6 and G8. Although chromatographic separation yielded a pure (+)-*trans*-*anti*-BP-modified oligomer, UV and circular dichroism characterization is not capable of differentiating between G6 and G8 adducts. The BP-H10 to BP-G8-H1′ NOE and the BP-H10 to C9-H1′ NOE (cross-peaks b and c in Figure 7A) place the BP-H10 proximate to the BP-G8-N^2 and show that G8 is the adduct site. The BP-H9 to C9-H1′ NOE interaction (cross-peak g in Figure 7C) and the NOE from BP-H8 to A16-H5′/H5″ (data not shown) further verify that BP is attached to G8 and define the orientation of the BP moiety with respect to the DNA helix.

The BP-H11 and BP-H12 protons exhibit NOEs to the A16-H2 proton (peaks e and f in Figure 7B) which places the BP-H11 and BP-H12 protons in the minor groove. The BP-H5/H6 aromatic protons on the outside edge of the BP chromophore exhibit NOEs to the A16-H4′, A16-H5′, and A16-H5″ protons (cross-peaks d, i, l, and m in Figure 8), which show that the BP moiety is directly above the A16 sugar and that the BP-H6 and BP-H5 protons are pointing out of the minor groove. NOEs between the BP-H1, BP-H3, and BP-H2 protons and the C17-H4′, C17-H5′, and C17-H5″ protons (cross-peaks a, b, c, f, j, and k in Figure 8) show that this end of the BP moiety is close to the C17 sugar.

NOE Distance Restraints. Eight of the BP to DNA NOE cross-peaks from a 150-ms mixing time NOESY spectrum recorded at 20 °C were used to determine distance restraints for restrained energy minimization and molecular dynamics calculations (Table 3). A biharmonic flat well penalty function with lower and upper bounds of 1.7−2.2 Å was employed for hydrogen bond restraints in the seven base pairs that exhibited evidence of Watson−Crick hydrogen bonding in the two-dimensional NOESY spectra and the terminal GC base pairs. Hydrogen bond restraints were not used for the T7·A16 and BP-G8·C15 base pairs since these partners did not exhibit the NOEs associated with Watson−Crick base pairing. As noted earlier, however, the chemical shifts of the T7 and BP-G8 imino protons as well as the base to H1′ and N-base to C-H5 NOEs, where N is the 5′ nucleotide, were consistent with Watson−Crick base pairing. The initial starting structure for energy minimization and molecular dynamics calculations had Watson−Crick base pairing for both T7·A16 and BP-G8·C15.

Energy Minimization and Molecular Dynamics Calculations. The protocol described in Materials and Methods was used to generate an energy-minimized structure that satisfied the BP to DNA distance restraints. The final energy-minimized structure is a B-type DNA (Figure 9) with a BP moiety attached in the minor groove at G8-N^2. Watson−Crick hydrogen bonding is observed for all base pairs in the BP-11-mer, including T7·A16 and BP-G8·C15. The BP moiety is oriented toward the 5′ end of the modified strand and is located near the A16 and C17 sugars on the partner strand.

In the energy-minimized structure all of the NOE distance restraints in Table 3 are within the upper and lower bounds. We note, however, that the observed distances for restraints 1−5 are shorter than the NOE-derived distances, although each is larger than the lower bound. We believe this is a result of the underestimation of the magnitude of the NOEs involving the A16 and C17 sugar protons due to line broadening observed with these resonances. As noted in Materials and Methods, we anticipated this problem and selected generous upper and lower bounds to minimize the potential of biasing the structure due to chemical exchange effects. As a check of the structure, the remaining BP to DNA NOE interactions were measured in the energy-minimized structure, and all proton pairs were within 5.0 Å, confirming that the energy-minimized structure (Figure 9) is consistent with all NMR data.

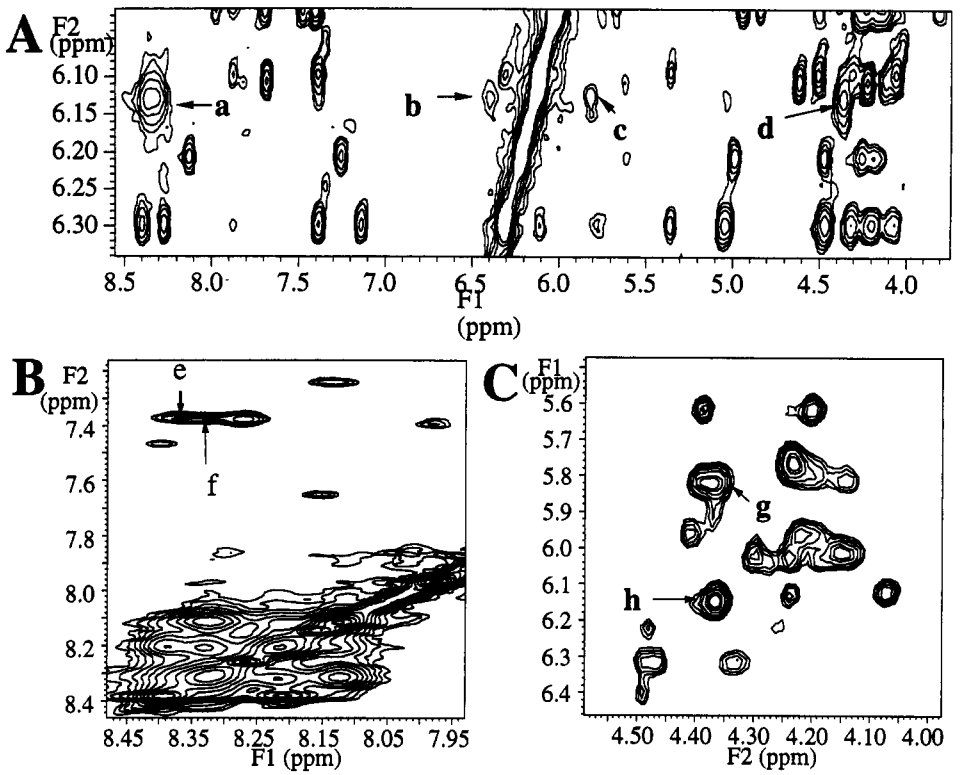

FIGURE 7: Portions of 400-ms NOESY spectra recorded at 20 °C showing interactions between BP aliphatic protons and BP-G8 , C9, and A16 nucleotide protons. The labeled cross-peaks are a, BP-H10 to BP-H11 and BP-H12; b, BP-H10 to BP-G8-H1′; c, BP-H10 to C9-H1′; d, BP-H10 to BP-H9; e, BP-H11 to A16-2H; f, BP-H12 to A16-2H; g, BP-H9 to C9-H1′; and h, BP-H10 to BP-H9.

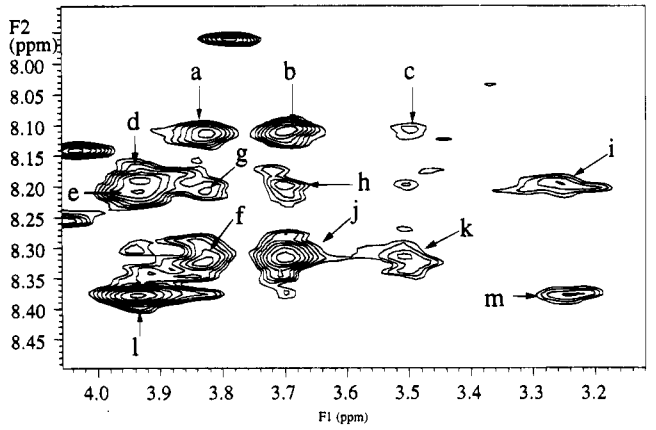

FIGURE 8: Portion of a 400-ms NOESY spectrum recorded at 20 °C showing close interactions between the aromatic protons and the A16 and C17 nucleotide protons. The labeled cross-peaks are a, BP-H2 to C17-H5′ or H5″; b, BP-H2 to C17-H4′; c, BP-H2 to C17-H5′ or H5″; d, BP-H5 to A16-H5′/H5″; e, BP-H4 to A16-H5′/H5″; f, BP-H1/H3 to C17-H5′ or H5″; g, BP-H4 to C17-H5′ or H5″; h, BP-H4 to C17-H4′; i, BP-H4/H5 to A16-H4′; j, BP-H1/H3 to C17-H4′; k, BP-H1/H3 to C17-H5′ or H5′; l, BP-H6 to A16-H5′ or H5″; and m, BP-H6 to A16-H4′.

Table 3: Experimental Distance Restraints Used in Energy Minimization Calculations and Observed Distances in the Lowest Energy Structure for the Predominant Conformer

	atom pair	lower bound (Å)	upper bound (Å)	calculated distance[a] (Å)	distance in structure[b] (Å)
1	BP-H6 to A16-H4′	2	5	3.7	2.7
2	BP-H5 to A16-H4′	2	5	3.9	2.8
3	BP-H2 to C17-H4′	2	5	4.2	3.6
4	BP-H12 to A16−2H	2	5	4.6	3.2
5	BP-H11 to A16−2H	2	5	4.4	2.9
6	BP-H9 to C9-H1′	2	3.5	2.5[c]	3.3
7	BP-H10 to C9-H1′	2.5	4.5	3.5	3.6
8	BP-H10 to G8-H1′	2.5	4.5	3.6	3.9

[a] Distances determined from a 150-ms NOESY spectrum recorded at 20 °C. [b] Distance measured in the lowest energy structure. [c] This cross-peak is partially overlapped with the C9-H1′ to C9-H4′ cross-peak.

DISCUSSION

In the *(+)-trans-anti*-BP-11-mer the BP moiety is covalently attached to G8-N^2 in the minor groove of a B-type duplex with Watson−Crick base pairing for all base pairs. The BP moiety is oriented toward the 5′ end of the modified strand and is located close to the C15-A16-C17 sugars on the partner strand. These important structural features are clearly defined by the NOE data. The chemical shifts observed in the NMR spectra of the BP-11-mer when compared to those in the unmodified 11-mer (Figure 6) also are consistent with the energy-minimized structure shown for the predominant conformer (Figure 9). The C15, A16, and C17 protons that are located in the shielding region of the BP chromophore exhibit large positive $\Delta\delta$ values. The A16 sugar protons that exhibit the largest upfield shifts are centered directly under the BP chromophore. The BP-G8-H1′ proton in the energy-minimized structure is in the plane of the BP chromophore, which is consistent with the $\Delta\delta$ value of −0.6 ppm. Although the presence of a conformational equilibrium limits the interpretation of the structure of the predominant conformer of the BP-11-mer in terms of specific molecular details, we believe that conformational equilibria may be an important feature of mutagenesis, as discussed below.

The predominant conformer of the BP-11-mer duplex, with a (...T[BP-G]C...)•(...GCA...) sequence, is similar to that reported by Cosman et al. (1992) for a (...C[BP-G]C...)•

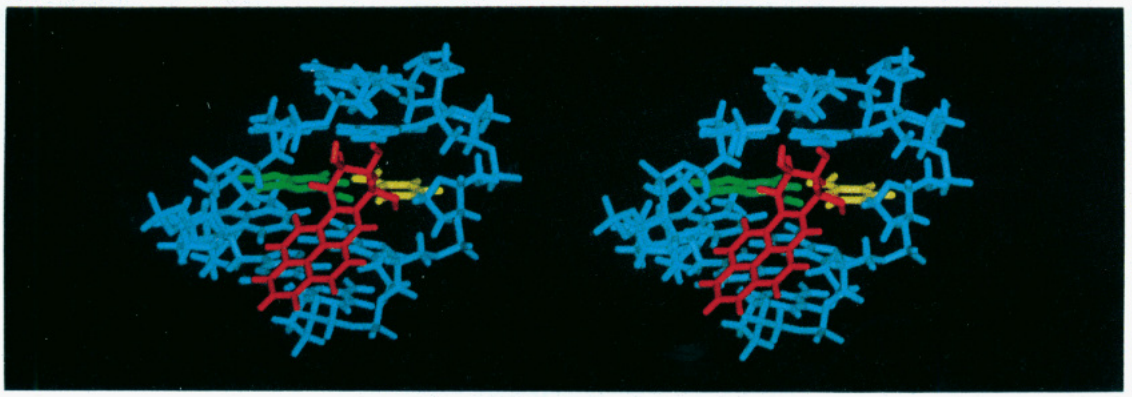

FIGURE 9: Stereo pairs of the d(G6-T7-[BP-G8]C9-A10)·(T13-G14-C15-A16-C17) section of the energy-minimized BP-11-mer duplex looking into the minor groove. The modified strand is on the left side of the duplex with the G6 base at the bottom of the strand and the A10 base at the top. The BP-G8 base is shown in green, the BP moiety is shown in red, and the C15 base on the partner strand is shown in yellow.

(...GCG...) sequence (the T and C bases are underlined to highlight the different 5′ neighboring bases). Cosman et al. (1992) did not report evidence of multiple conformers for their (...C[BP-G]C...)·(...GCG...) modified duplex, which contrasts with the interconversion of a predominant conformer and a minor conformer described above for the BP-11-mer duplex. Apparently, the presence of the 5′ T on the modified strand in the BP-11-mer gives rise to a minor conformer, which illustrates the effect of sequence on conformational equilibrium.

The presence of the BP moiety in the minor groove of a B-type duplex for the predominant conformer provides a visualization of an adduct structure that could allow faithful replication of the modified strand. It does not, however, provide an obvious structural basis for rationalizing the mutagenesis observed with (+)-*trans-anti*-BP adducts. In this regard, the structural heterogeneity observed in the present experiments may be an important aspect of the mutagenesis of BP. The presence of a T·A base pair on the 5′ side of the BP modification site has been shown to have an impact on mutagenesis (Mackay et al., 1992; Shibutani et al., 1993). Loechler and co-workers (Mackay et al., 1992; Rodriguez & Loechler, 1993a) have proposed that BP adducts can adopt multiple conformations and that each of the conformers can cause a different pattern of mutation. The present experiments lend support to a correlation between structure and mutagenesis, although establishing a direct correlation requires further studies.

In spite of extended efforts, we were unable to slow the interconversion between conformers sufficiently to obtain NOE-derived distances from the minor conformer. The line broadening observed for the T7 and G8 imino protons, when coupled with enhanced solvent exchange for these imino protons compared to adjacent imino protons (Figure S2, in supplementary material), is suggestive of a distortion of the BP-11-mer at this location. The line broadening of the C17-H6 and C17-H5 protons suggests that in the minor conformer the BP moiety has moved with respect to these protons. We anticipate that significant structural rearrangements are involved [e.g., see the aminofluorene equilibrium in Eckel and Krugh (1994a,b)]. The hydrophobic nature of the BP moiety leads to the suggestion that the minor conformer involves insertion of the BP moiety into the duplex, with disruption of Watson−Crick base pairing. Although such a structure would provide a visualization of a premutagenic conformation, and is consistent with the limited data we have on the conformational equilibrium, we caution that this is only a working hypothesis because the lack of NOE data for the minor conformer of the BP-11-mer duplex precludes a characterization of its solution conformation.

Concluding Remarks. The study of the d(T[BP-G]C) lesion shows that more than one conformation exists for the (+)-*trans-anti*-BP-dG adduct bound at this sequence. Conformational equilibria have been observed in other carcinogen-modified duplexes [e.g., O'Handley (1991), O'Handley et al. (1992, 1993), Cosman et al. (1993), and Eckel and Krugh (1994a,b)] and may be an important factor in mutagenesis. For example, an aminofluorene-modified DNA oligomer exhibited a conformational equilibrium between two structures (Eckel & Krugh, 1994a,b) in which one conformation exhibits Watson−Crick base pairing of the AF-G·C pair, whereas the second conformer exhibits disruption of this base pair and insertion of the fluorene moiety into the duplex. By analogy, it is interesting to propose that an equivalent conformational equilibrium is involved when BP is bound at a TGC sequence.

ACKNOWLEDGMENT

We thank our colleagues Charles Bailey and Linda Eckel for many useful discussions.

SUPPLEMENTARY MATERIAL AVAILABLE

Circular dichroism and absorption spectra of the (−)-*trans-anti*-BP-dG adduct and the (+)-*trans-anti*-BP-dG adduct (Figure S1), a graph of the exchange rates of the imino protons at −5 °C (Figure S2), two-dimensional NOESY spectra of the base to H1′ region recorded at 5, 10, 20, and 37 °C (Figure S3), two-dimensional NOESY and TOCSY spectra recorded at 20 °C showing the BP proton assignments (Figures S4 and S5), chemical shifts of the unmodified 11-mer (Table S1), and a summary of BP to DNA NOEs (Table S2) (7 pages). Ordering information is given on any current masthead page.

REFERENCES

Burgess, J. A., Steven, C. W., & Fahl, W. E. (1985) *Cancer Res. 45*, 4257−4262.

Cheng, S. C., Hilton, B. D., Roman, J. M., & Dipple, A. (1989) *Chem. Res. Toxicol. 2*, 334−340.

Cho, B. P., Beland, F. A., & Marques, M. M. (1994) *Biochemistry 33*, 1373−1384.
Chou, S.-H., Flynn, P., & Reid, B. (1989) *Biochemistry 28*, 2435−2443.
Conney, A. H. (1982) *Cancer Res. 42*, 4875−4917.
Cosman, M., Ibanez, V., Geacintov, N. E., & Harvey, R. G. (1990) *Carcinogenesis 11*, 1667−1672.
Cosman, M., de los Santos, C., Fiala, R., Hingerty, B. E., Singh, S. B., Ibanez, V., Margulis, L. A., Live, D., Geacintov, N. E., Broyde, S., & Patel, D. J. (1992) *Proc. Natl. Acad. Sci. U.S.A. 89*, 1914−1918.
Cosman, M., de los Santos, C., Fiala, R., Hingerty, B. E., Ibanez, V., Luna, E., Harvey, R., Geacintov, N. E., Broyde, S., & Patel, D. J. (1993) *Biochemistry 32*, 4145−4155.
Cosman, M., Fiala, R., Hingerty, B. E., Amin, S., Geacintov, N. E., Broyde, S., & Patel, D. J. (1994) *Biochemistry 33*, 11507−11517.
de los Santos, C., Cosman, M., Hingerty, B. E., Ibanez, V., Margulis, L. A., Geacintov, N. E., Broyde, S., & Patel, D. J. (1992) *Biochemistry 31*, 5245−5252.
Early, T. A., Feigon, J., & Kearns, D. R. (1980) *J. Magn. Reson. 41*, 343−348.
Eckel, L. M., & Krugh, T. R. (1994a) *Nature Struct. Biol. 1*, 89−94.
Eckel, L. M., & Krugh, T. R. (1994b) *Biochemistry 33*, 13611−13624.
Folta-Stogniew, E., & Russu, I. M. (1994) *Biochemistry 33*, 11016−11024.
Fountain, M. A. (1994) Structural Characterization of the d(CCTATGT[(+)-*trans-anti*-BP-G]CAC):d(GTGCACAT-AGG) Oligonucleotide Duplex Using NMR and Molecular Modeling, Ph.D. Dissertation, University of Rochester, Rochester, NY.
Galat, A. (1990) *Eur. Biophys. J. 17*, 331−342.
Geacintov, N. E., Cosman, M., Ibanez, V., Birke, S. S., & Swenberg, C. E. (1990) Characteristics of Noncovalent and Covalent Interactions of (+) and (−) *anti*-Benzo[a]pyrene Diol Epoxide Stereoisomers of Different Biological Activities with DNA, in *Molecular Basis of Specificity in Nucleic Acid-Drug Interactions*, pp 433−450, Kluwer Academic Publishers, Dordrecht.
Gelbion, H. V. (1980) *Physiol. Rev. 60*, 1107−1166.
Glatt, H., Seidel, A., Bochnitschek, W., Marquardt, H., Hodgson, R. S., Grover, P. L., & Oesch, F. (1986) *Cancer Res. 46*, 4556−4565.
Harvey, R. G. (1991) *Polycyclic aromatic hydrocarbons: chemistry and carcinogenicity*, Cambridge University Press, Cambridge.
Hore, P. J. (1983) *J. Magn. Reson. 55*, 283−300.
Jernstrom, B., & Graslund, A. (1994) *Biophys. Chem. 49*, 185−199.
Mackay, W., Benasutti, M., Drouin, E., & Loechler, E. L. (1992) *Carcinogenesis 13*, 1415−1425.
Mirau, P. A., & Bovey, F. A. (1987) *J. Magn. Reson. 71*, 201−211.
O'Handley, S. F. (1991) Structural Analysis of a Carcinogen-Modified DNA Oligomer by NMR Spectroscopy, Ph.D. Thesis, University of Rochester.
O'Handley, S. F., Sanford, D. G., Xu, R., Lester, C. C., Hingerty, B. E., Broyde, S., & Krugh, T. R. (1992) Structure of an Acetylaminofluorene (AAF) Modified DNA Oligomer, in *Structure & Function, Volume I: Nucleic Acids*, pp 137−145, Adenine Press, Schenectady, NY.
O'Handley, S. F., Sanford, D. G., Xu, R., Lester, C. C., Hingerty, B. E., Broyde, S., & Krugh, T. R. (1993) *Biochemistry 32*, 2481−2497.
Osborne, M. R., Jacobs, S., Harvey, R. G., & Brookes, P. (1981) *Carcinogenesis 2*, 553−558.
Pulkrabek, P., Leffler, S., Grunberger, D., & Weinstein, I. B. (1979) *Biochemistry 18*, 3127−3132.
Rodriguez, H., & Loechler, E. L. (1993a) *Biochemistry 32*, 1759−1769.
Rodriguez, H., & Loechler, E. L. (1993b) *Carcinogenesis 14*, 373−383.
Shibutani, S., Margulis, L. A., Geacintov, N. E., & Grollman, A. P. (1993) *Biochemistry 32*, 7531−7541.
Singh, S. B., Hingerty, B. E., Singh, U. C., Greenberg, J. P., Geacintov, N. E., & Broyde, S. (1991) *Cancer Res. 51*, 3482−3492.
Singh, U. C., Weiner, P. K., Caldwell, J., & Kollman, P. C. (1988) *AMBER Version 3.1*, University of California, San Francisco.
Sklenar, V., & Bax, A. (1987) *J. Magn. Reson. 74*, 469−479.
Thakker, D. R., Yagi, H., Levin, W., Wood, A. W., Conney, A. H., & Jerina, D. M. (1985) Polycyclic Aromatic Hydrocarbons: Metabolic Activation to Ultimate Carcinogens, in *Bioactivation of Foreign Compounds*, pp 177−242, Academic Press, New York.
Weiner, S. J., Kollman, P. A., Case, D. A., Singh, U. C., Ghio, C., Alagona, G., Profeta, S., Jr., & Weiner, P. (1984) *J. Am. Chem. Soc. 106*, 765−784.
Weiner, S. J., Kollman, P. A., Nguyen, D. J., & Case, D. A. (1986) *J. Comp. Chem. 7*, 230−252.

BI942361V